EUR 24.e

EUROPEAN ATOMIC ENERGY COMMUNITY – EURATOM

FINE FLUX MEASUREMENTS ON CONCENTRIC ANNULI FUEL ELEMENTS

by

R. BONALUMI and G.B. ZORZOLI

1962

RESEARCH AND DEVELOPMENT PROGRAM
EURATOM-CANADA

Special Technical Progress Report No R 45
established by CISE - Centro Informazioni Studi Esperienze
under the Euratom Contract No 012-60.12 Orgi

LEGAL NOTICE

This document was prepared under the sponsorship of the Commission of the European Atomic Energy Community (Euratom).

Neither the Euratom Commission, its contractors nor any person acting on their behalf:

1° — Make any warranty or representation, express or implied, with respect to the accuracy, completeness, or usefulness of the information contained in this document, or that the use of any information, apparatus, method, or process disclosed in this document may not infringe privately owned rights; or

2° — Assume any liability with respect to the use of, or for damages resulting from the use of any information, apparatus, method or process disclosed in this document.

This report can be obtained, at the price of Belgian Francs 50, from: PRESSES ACADEMIQUES EUROPEENNES, 98, chaussée de Charleroi, Brussels (Belgium).

Please remit payments:

— to BANQUE DE LA SOCIETE GENERALE (Agence Ma Campagne) account No. 964.558,

— to BELGIAN AMERICAN BANK and TRUST COMPANY - New York - account No 121.86,

— to LLOYDS BANK (Foreign) Ltd. - 10 Moorgate - London E.C. 2,

giving the reference: "EUR 24.e — Fine Flux Measurements on Concentric Annuli Fuel Elements".

Printed by Snoeck-Ducaju & Zoon. Brussels-Ghent. August 1962.

EUR 24.e

FINE FLUX MEASUREMENTS ON CONCENTRIC ANNULI FUEL ELEMENTS
by R. BONALUMI and G.B. ZORZOLI

European Atomic Energy Community - EURATOM.
Centro Informazioni Studi Esperienze - CISE.
Special Technical Progress Report on contract No. 012-60.12 ORGI.
Brussels, August 1962 - Pages 13 - Fig. 11.

This report describes two fine flux measurements on concentric annuli natural uranium fuel elements, containing a hydrogeneous material.

Two different fuel elements, with different uranium content and geometry and different hydrogen content, were tested on the Aquilon II facility. Neutron detectors were metal dysprosium disks placed into the aforesaid fuel elements.

The experimental results are compared with the theoretical ones, calculated by means of Amouyal and Benoist's theory: the agreement is quite satisfactory.

EUR 24.e

FINE FLUX MEASUREMENTS ON CONCENTRIC ANNULI FUEL ELEMENTS
by R. BONALUMI and G.B. ZORZOLI

European Atomic Energy Community - EURATOM.
Centro Informazioni Studi Esperienze - CISE.
Special Technical Progress Report on contract No. 012-60.12 ORGI.
Brussels, August 1962 - Pages 13 - Fig. 11.

This report describes two fine flux measurements on concentric annuli natural uranium fuel elements, containing a hydrogeneous material.

Two different fuel elements, with different uranium content and geometry and different hydrogen content, were tested on the Aquilon II facility. Neutron detectors were metal dysprosium disks placed into the aforesaid fuel elements.

The experimental results are compared with the theoretical ones, calculated by means of Amouyal and Benoist's theory: the agreement is quite satisfactory.

EUR 24.e

FINE FLUX MEASUREMENTS ON CONCENTRIC ANNULI FUEL ELEMENTS
by R. BONALUMI and G.B. ZORZOLI

European Atomic Energy Community - EURATOM.
Centro Informazioni Studi Esperienze - CISE.
Special Technical Progress Report on contract No. 012-60.12 ORGI.
Brussels, August 1962 - Pages 13 - Fig. 11.

This report describes two fine flux measurements on concentric annuli natural uranium fuel elements, containing a hydrogeneous material.

Two different fuel elements, with different uranium content and geometry and different hydrogen content, were tested on the Aquilon II facility. Neutron detectors were metal dysprosium disks placed into the aforesaid fuel elements.

The experimental results are compared with the theoretical ones, calculated by means of Amouyal and Benoist's theory: the agreement is quite satisfactory.

EUR 24.e

EUROPEAN ATOMIC ENERGY COMMUNITY – EURATOM

FINE FLUX MEASUREMENTS ON CONCENTRIC ANNULI FUEL ELEMENTS

by

R. BONALUMI and G.B. ZORZOLI

1962

RESEARCH AND DEVELOPMENT PROGRAM
EURATOM-CANADA

Special Technical Progress Report No R 45
established by CISE - Centro Informazioni Studi Esperienze
under the Euratom Contract No 012-60.12 Orgi

CONTENTS

KEY TO THE TABLES

KEY TO THE FIGURES

FINE FLUX MEASUREMENTS ON CONCENTRIC ANNULI FUEL ELEMENTS

SUMMARY

This report describes two fine flux measurements on concentric annuli natural uranium fuel elements, containing a hydrogeneous material.

Two different fuel elements, with different uranium content and geometry and different hydrogen content, were tested on the Aquilon II facility. Neutron detectors were metal dysprosium disks placed into the aforesaid fuel elements.

The experimental results are compared with the theoretical ones, calculated by means of Amouyal and Benoist's theory: the agreement is quite satisfactory.

1 — INTRODUCTION

Within the frame of a general experimental program concerning heavy water moderated lattices with concentric annuli natural uranium fuel elements, some fine flux measurements have been performed, at the Aquilon II critical facility.

These measurements were aimed at providing experimental information about such lattices, so that a comparison could be made with the adopted theory for thermal utilization factor[1], in order to achieve a confident know-how on power distribution inside fuel elements.

What has been done gives good evidence of quite a satisfactory agreement between theory and experiments, also showing interesting features of hydrogenized fuel elements, which could be exploited in a power reactor design.

2 — SUMMARY OF PRELIMINARY WORK

Two problems were to be faced: 1) the choice of a solid hydrogeneous material with a hydrogen concentration flexible enough so as to simulate water-steam mixtures at different densities; 2) the choice of detectors whose epithermal neutron activation was either negligeable when compared to thermal or reliably related to known lattice characteristics.

A hydrogeneous material fulfilling our requirements was found to be expanded polistyrene: several chemical analyses showed a high nuclear purity.

Among the different possible densities two were chosen as most suitable, i.e. about 0.300 and 0.600 g/cm^3.

As for the detector material, natural dysprosium appeared to be just what was needed, due to the rigorously $1/v$ absorption cross section of Dy^{164} isotope, whose activation product (Dy^{165}) is the only one β^- decaying among all Dy isotopes.

20 Dy detectors, 4 mm in diameter, 0.06 mm thick, were calibrated by counting in three double G.M. - tube chains, after a standard irradiation under a Ra-Be source.

Listed in Table I are the relative detector efficiencies; the efficiency of the nth detector is defined as the 4th to the nth detector calibration counting ratio.

3 — EXPERIMENTAL ARRANGEMENT

Two configurations were the object of fine flux measurements; they are referred to as follows:

AC-2-T-1-21: fuel element as shown in Fig. 1, with low density polistyrene (0.271 g/cm³); lattice pitch = 21 cm.

AC-1-T-3-24: fuel element as shown in Fig. 2, with high density polistyrene (0.511 g/cm³); lattice pitch = 24 cm.

Because of the gap existing between fuel annuli and polistyrene pieces due to the manufacturing tolerances, the polistyrene densities hereupon stated are the actual ones diluted over the whole regions indicated in Fig. 1 and 2 as "hydrogeneous medium regions".

Two irradiations have been performed for either configuration, so as to avoid any self-shielding effect between detectors: to normalize the activations, some positions have been provided with detectors during both irradiations.

Figs. 3 to 6 illustrate the detector positions during the different irradiations; in all the figures, the number above the detector represents its order number as stated in table I, while radii are quoted below in mm.

The experimental arrangement is also shown in Fig. 7, which is a picture of the portion of the AC-2-T-1 fuel element where detectors were positioned: some of them appear placed in their own slots.

Fig. 8 is a picture showing, for the sake of comparison, uranium and polistyrene pieces along with *Dy* detectors and aluminum holders.

Such technique allowed detectors to be extracted from the fuel element in ten minutes, so that such operation could be performed about ten minutes after the irradiation was over, without any harm for the personnel charged with disassemblying such elements.

It is also worth noting that detectors placed into polistyrene were bare, whereas the ones held by uranium were 1/10 mm thick aluminium-covered, to prevent any fission product contamination.

In the case of the configuration AC-2-T-1-21, the special fuel element was positioned as shown in Fig. 9-a, i.e. in one of the four central positions, 16 elements of the reference lattice being replaced by AC-2-T-1 elements.

In the case of the configuration AC-1-T-3-24, the special fuel element, always in one of the four central positions (Fig. 9-b), was part of a replacement set of 24 AC-1-T-3 elements. Irradiation was performed by reactor divergence up to 25 *W*, and lasted about half an hour, in all of the four cases shown in Figs. 3 through 6. The special elements being in the center of the lattice, it is sensible to assume that the neutron energy spectrum be actually the same as in a critical uniform lattice fully consisting of fuel elements of the type under study.

Detectors were counted in 8 counting chains: the collected count values, automatically punched, fed a 7090 IBM computer, along with a code which gives as output the net counting rate (counts per minute) corrected for dead time, counter and detector efficiency, etc.

It is worthwhile to recall that each irradiation involved 10 detectors, whereas the counting chains were 8. For this reason, 2 counting runs were necessary, each of them covering 8 detectors; then 6 detectors were counted twice, thus achieving a better statistics.

4 — EXPERIMENTAL RESULTS

Tables II and III list the activation values for AC-2-T-1-21 and AC-1-T-3-24 configurations respectively: values are already normalized to unity on the axis of the element, and are corrected for counting chains and detector efficiency, delay-time between irradiation and counting, axial position of detectors inside fuel element, and so on. For positions where more than one activation value was available, only the average value is quoted, since differences between single data were within the experimental errors. The latter are not quoted; the standard deviation of single measurements was ranging between 0.35 and 0.37 %, neglecting uncertainties in position. The latter are different in uranium and in polistyrene; in fact:

a) for uranium slots ($\sim$ 25/100 mm wide), the uncertainty depends essentially upon the reading by means of a vernier slide gage, and can be estimated of about 1/10 mm; the presence of the aluminum cover to protect detectors against fission products makes the *Dy* position rather sure;

b) for slots in polistyrene ($\sim$ 3/10 mm wide), besides the gage reading uncertainty increased by possible polistyrene shifting due to the tolerances, allowance should be made for the intrinsic uncertainty in position, arising from their being fairly thicker (2-3/10 mm to be compared with 6/100 mm) than *Dy* detectors, which are bare.

On the other hand, in order to get average flux values in the different regions, integrations were needed over every region, and the drawing of a smooth line, as close as possible to the experimental point values, looked as the most acceptable way of doing this.

The adjusted flux line exhibits a deviation from experimental data always within about 2 % (Figs. 10 and 11), which nevertheless is higher than the intrinsic experimental uncertainties.

Only one point exhibits a larger deviation, that is the point at $r = 27.5$ mm in AC-2-T-1-21 irradiation (see Fig. 10): this point was actually disregarded in drawing the fitting line. Since radially symmetrical detectors showed no appreciable maseroscopic flux effect, no correction was made for that.

5 — EVALUATION OF REGION AVERAGED FLUXES

A convenient way of averaging fluxes over single regions was deemed to be based upon Gauss' formula, applied to the flux fitting line.

If a_i, b_i are the inner and outer radius of the i^{th} region, its average flux $\overline{\varphi_i}$ is by definition:

$$\overline{\varphi_i} = \frac{2}{b^2{}_i - a^2{}_i} \int_{a_i}^{b_i} r\,\varphi(r)\,dr$$

Now, if one assumes the function $r\varphi(r)$, which is quite a smooth one, to be well represented within each region by a 5th degree polynomial of r, then Gauss' formula provides the following result:

$$\overline{\varphi_i} = \frac{2}{a_i + b_i}\left\{\frac{5}{18}\left[y(r_1) + y(r_3)\right] + \frac{4}{9}y(r_2)\right\}$$

where:

$$y(r) = r\,\varphi(r)$$

$$r_1 = a_i + 0.1127(b_i - a_i)$$

$$r_2 = \frac{a_i + b_i}{2}$$

$$r_3 = a_i + 0.8873(b_i - a_i)$$

6 — COMPARISON WITH THEORY

Experimental region averaged fluxes have been compared with theoretical results calculated after Amouyal and Benoist's generalized theory [1].

An important item to be pointed out is that theoretical calculations have been carried out for a *thermal* neutron population.

On the other hand, due to the $1/v$ trend of *Dy* activation cross section, measured activities are actually proportional to the *total* neutron *densities* so that, in order for a comparison to be made between theoretical and experimental *thermal* neutron densities, the detector activities should be corrected for the epithermal contribution.

For lack of time, no measurement was possible with Cd-covered detectors, so that what has been done here follows a slightly different line, which is largely sufficient, at any rate, for an effective comparison between theory and experiments, and thus for drawing some general conclusions.

Let:

n_{exp} = total experimental neutron density normalized to $\bar{n}_{exp,1} = 1$ in the innermost region

n_{th} = thermal theoretical neutron density with $\bar{n}_{th,1} = 1$ in the innermost region

n_e = epithermal neutron density, assumed constant throughout the cell.

The quantity n_e is evaluated from macroscopic considerations.

Let:

ε = fast fission factor;

f = thermal utilization factor;

η = thermal fission factor;

$\bar{\Sigma}_{aCM}$ = overall cell thermal absorption macroscopic cross section (maxwellian averaged value);

$\bar{\Sigma}^*_{sCe}$ = overall cell epithermal slowing-down macroscopic cross section ($1/E$ spectrum averaged);

B^2 = material buckling;

$\bar{v}_M$ = thermal neutron average velocity;

$\bar{v}_e$ = epithermal neutron average velocity;

v_o = 2200 m/s

All quantities have been theoretically calculated, except for B^2 (experimental), and the results listed in Table IV, referring to both configurations tested, are derived from Ref. 2.

The epithermal to thermal overall density ratio was calculated for either case by the formula:

$$\left(\frac{n_e}{n_{th}}\right)_{cell} = \frac{\bar{v}_M}{\bar{v}_e} \frac{\varepsilon f \eta}{1 + B^2 L^2_e} \frac{\bar{\Sigma}_{aCM}}{\bar{\Sigma}^*_{sCe}}$$

Once $\left(\frac{n_e}{n_{th}}\right)_{cell}$ is known, one gets immediately the total calculated neutron density (normalized to one in the innermost region)

$$n_{calc} = \frac{n_{th} + n_e}{1 + n_e}$$

The quantities n_{exp}, n_{th}, n_{calc}, along with the percent error $100 \frac{n_{calc} - n_{exp}}{n_{exp}}$, are listed for both elements in Table V, for all the regions involved in the present experimental investigation.

As can be seen from listed data, the agreement between theory and experiments is satisfactory. As a conclusion, the adopted theory for calculating f can be recognized as adequate enough so as to be safely accepted in reactor physics design calculations.

7 — CONCLUSIONS

Experimental measurements demonstrate the following facts:

a) Agreement between theory and experiments is satisfactory enough so as to allow future theoretical studies of good reliability.

b) Some interesting features of hydrogen moderation are worth emphasizing. As can be seen from Fig. 11 (AC-1-T-3-24 flux plot), the behavior of polistyrene is to a certain extent dependent upon where the hydrogeneous medium is placed. More precisely, if polistyrene is close to moderator on one side, and to fuel on the other one, capture characteristics prevail over the moderating ones, as is well shown by the nearly straight

increase of flux outwards. The opposite happens when polistyrene is surrounded by uranium on both sides: in this case, the flux downward concavity proves that hydrogen acts mainly as a thermal neutron source, i.e. its moderating properties prevail over the parasitic ones. Something intermediate is the result in the central cylinder, where source effects are but slightly prevailing over sink effects, because of the relatively large volume of material. The aforesaid conclusions are confirmed by inspection of Fig. 10.

As a conclusion, withdrawal or injection of a hydrogeneous coolant (i.e. what polistyrene stands for in experiments) into coolant channels, may produce quite different effects, depending upon the position where it takes place and the volume involved in the perturbation: thus, a more extensive fine distribution study, theoretical and experimental, on hydrogen effects, seems to be pretty interesting.

REFERENCES

(1) AMOUYAL A., BENOIST P., GUIONNET C. — *Calcul du facteur d'utilisation thermique dans une cellule formée d'un nombre quelconque de milieux concentriques* — Rapport CEA 1967 (1961).

(2) BONALUMI R., ZORZOLI G.B. — *Final report on heavy water lattice buckling measurements* — Euratom Report EUR. 25. e (1962).

Table I

DYSPROSIUM DETECTORS EFFICIENCY

Detector number	1	3	4	5	6	7	8
Efficiency	1.0051±0.0032	0.9110±0.0029	1.0000±0.0033	1.0164±0.0033	0.9260±0.0030	0.9281±0.0029	0.9733±0.0031
Detector number	9	10	11	12	13	14	15
Efficiency	0.9475±0.0030	0.9836±0.0031	0.9416±0.0030	0.9488±0.0030	0.9322±0.0029	0.9907±0.0032	0.9118±0.0029
Detector number	16	17	18	19	20	21	
Efficiency	0.9155±0.0029	0.9015±0.0028	0.9158±0.0029	0.9009±0.0028	0.9225±0.0029	0.9076±0.0029	

Table II

AC-2-T-1-21 ACTIVATION VALUES

r (mm)	Material	Activation
0	U	1.0000
5.5	U	1.0354
9.5	U	1.1455
13.5	U	1.2460
16.7	CH	1.5030
19.6	CH	1.6454
20.7	CH	1.6708
21.5	CH	1.6728
23.5	U	1.7408
27.5	U	2.0963
28.6	CH	1.9973
30.5	CH	2.3344
32.3	CH	2.5706
32.4	CH	2.6237

Table III

AC-1-T-3-24 ACTIVATION VALUES

r (mm)	Material	Activation
0	CH	1.0000
5.5	CH	1.0049
9.5	CH	0.9910
11.0	CH	0.9517
12.5	U	0.9227
16.0	U	0.9778
16.8	CH	0.9866
18.3	CH	1.0715
20.3	CH	1.0883
22.2	CH	1.0922
23.5	U	1.0919
27.5	U	1.2630
28.8	CH	1.3100
30.5	CH	1.4508
32.2	CH	1.6882

Table IV

MACROSCOPIC PARAMETERS FOR BOTH TESTED CONFIGURATIONS

	AC-2-T-1-21	AC-1-T-3-24
T_n	40.8 °C	33.1 °C
ε	1.0414	1.0322
f	0.9416	0.9110
η	1.3190	1.3202
$\overline{\Sigma}_{aCM}$ (cm^{-1})	0.5535×10^{-2}	0.3756×10^{-2}
$\bar{\nu}_M/v_o$	1.1668	1.1525
$\frac{\bar{\nu}_o}{v_o}\overline{\Sigma}^{*}_{sCe}$ (cm^{-1})	0.1955	0.2074
B^2 (cm^{-2})	5.70×10^{-4}	4.13×10^{-4}
L^2_o (cm^2)	121.66	112.78
$\frac{n_e}{n_{th}}$	0.03996	0.02476

Table V

EXPERIMENTAL AND THEORETICAL AVERAGE NEUTRON DENSITIES

AC-2-T-1-21 configuration

Region	Material	n_{exp}	n_{th}	$n_{calc} = \frac{n_{th}+0.1273}{1.1273}$	$\frac{n_{calc}-n_{exp}}{n_{exp}}100$
1	U	1.000	1.000	1.000	0
2	CH	1.354	1.472	1.419	+ 4.8
3	U	1.551	1.626	1.555	+ 0.3
4	CH	1.915	2.144	2.015	+ 5.2

AC-1-T-3-24 configuration

Region	Material	n_{exp}	n_{th}	$n_{calc} = \frac{n_{th}+0.06291}{1.06291}$	$\frac{n_{calc}-n_{exp}}{n_{exp}}100$
1	CH	1.000	1.000	1.000	0
2	U	0.952	0.947	0.950	— 0.2
3	CH	1.092	1.167	1.157	+ 5.9
4	U	1.194	1.250	1.235	+ 3.4
5	CH	1.521	1.655	1.616	+ 6.2

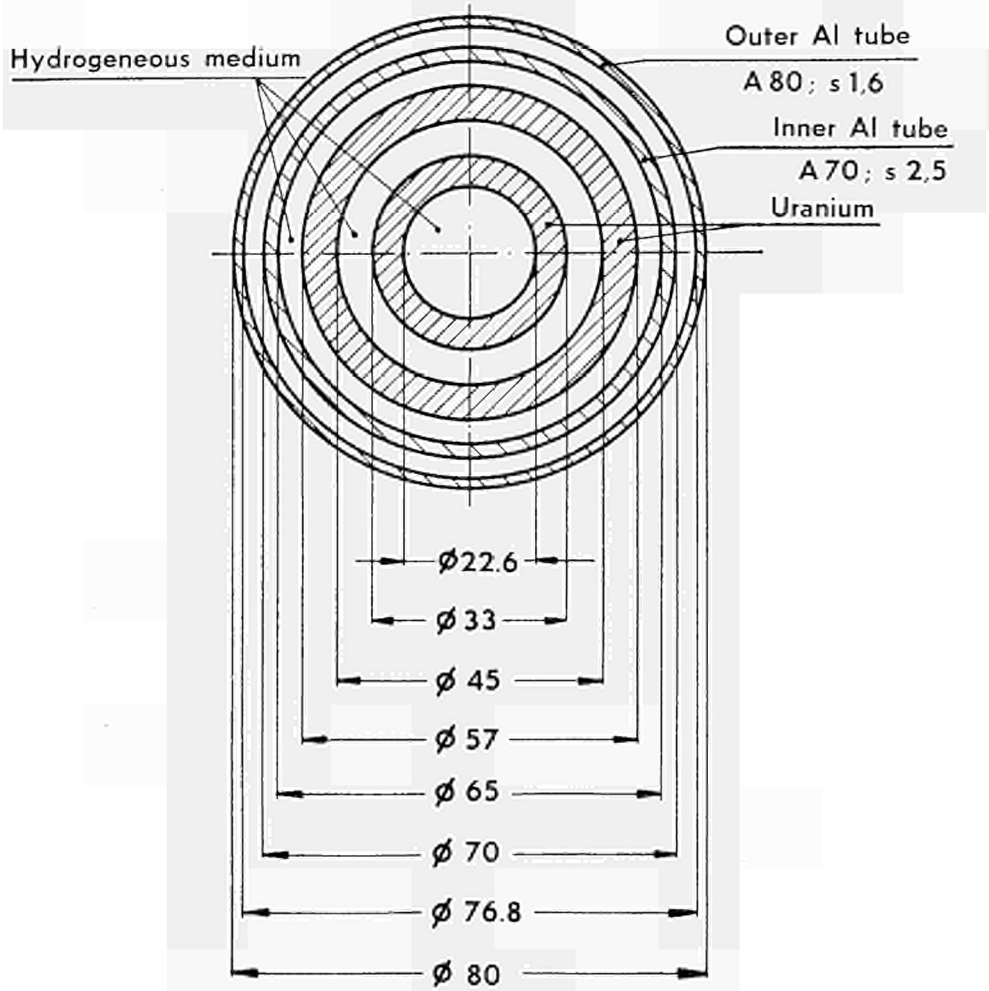

Fig. 1 — *AC-2 Fuel element cross section.*

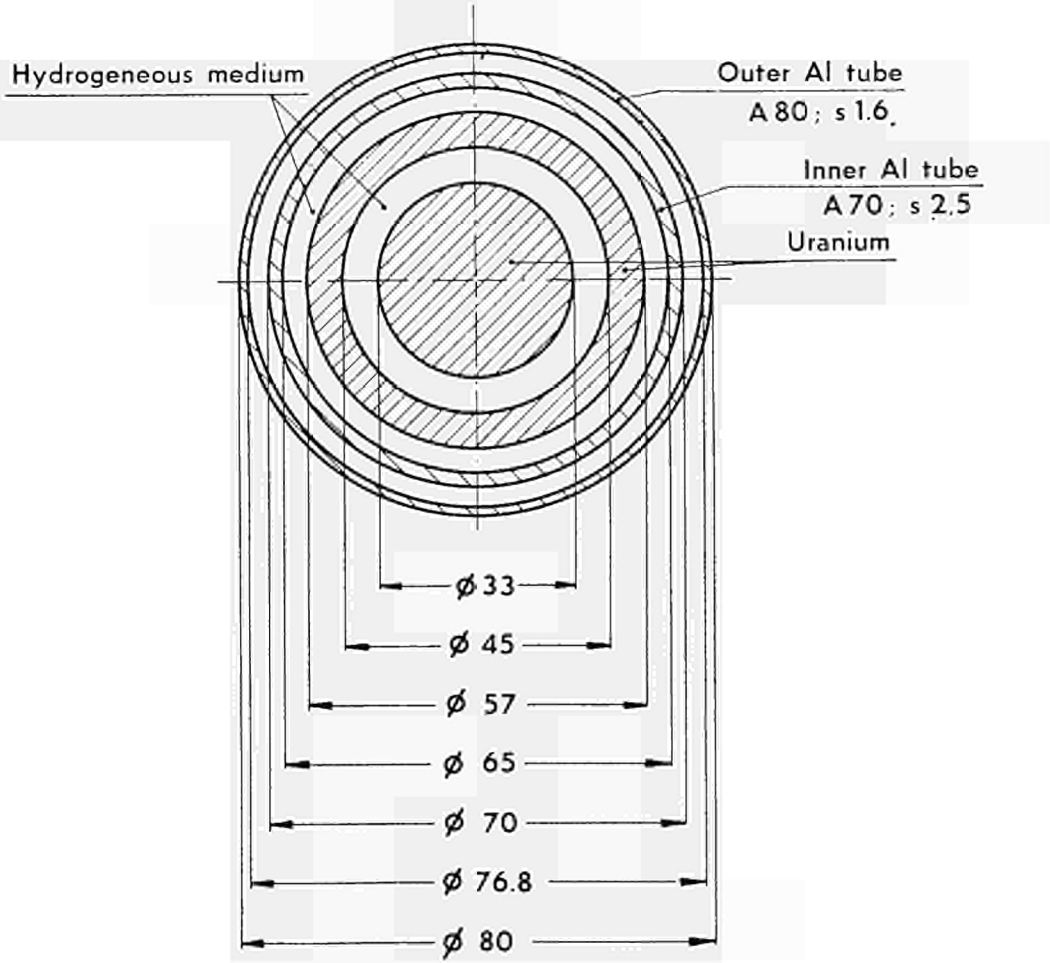

Fig. 2 — *AC-1 Fuel element cross section.*

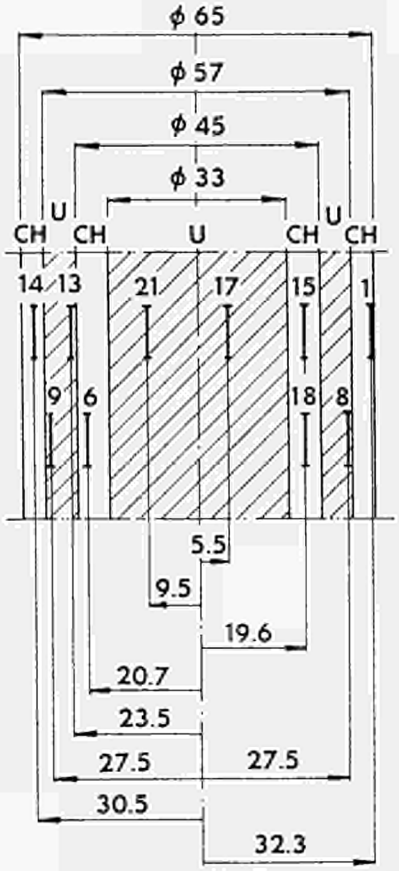

Fig. 3 — *AC-2-T-1-21 1st irradiation: detector position.*

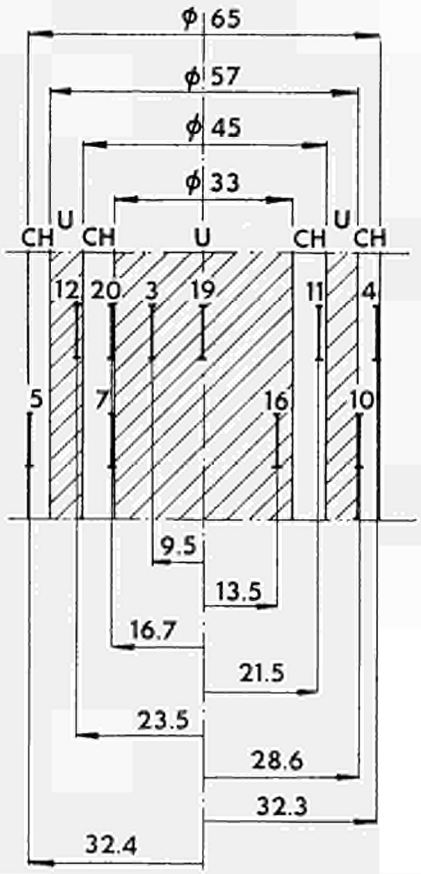

Fig. 4 — *AC-2-T-1-21 2nd irradiation: detector position.*

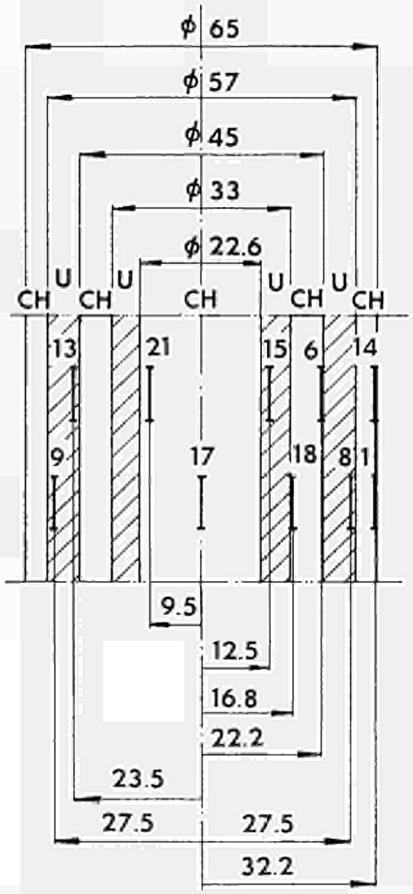

Fig. 5 — *AC-1-T-3-24 1st irradiation: detector position.*

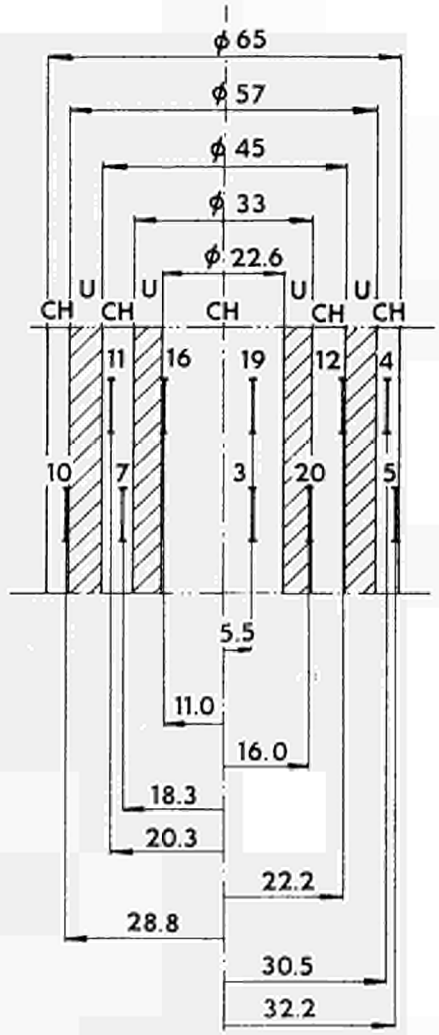

Fig. 6 — *AC-1-T-3-24 2nd irradiation: detector position.*

Fig. 7. — AC-2-T-1 element: section holding detectors (some are visible in their slots).

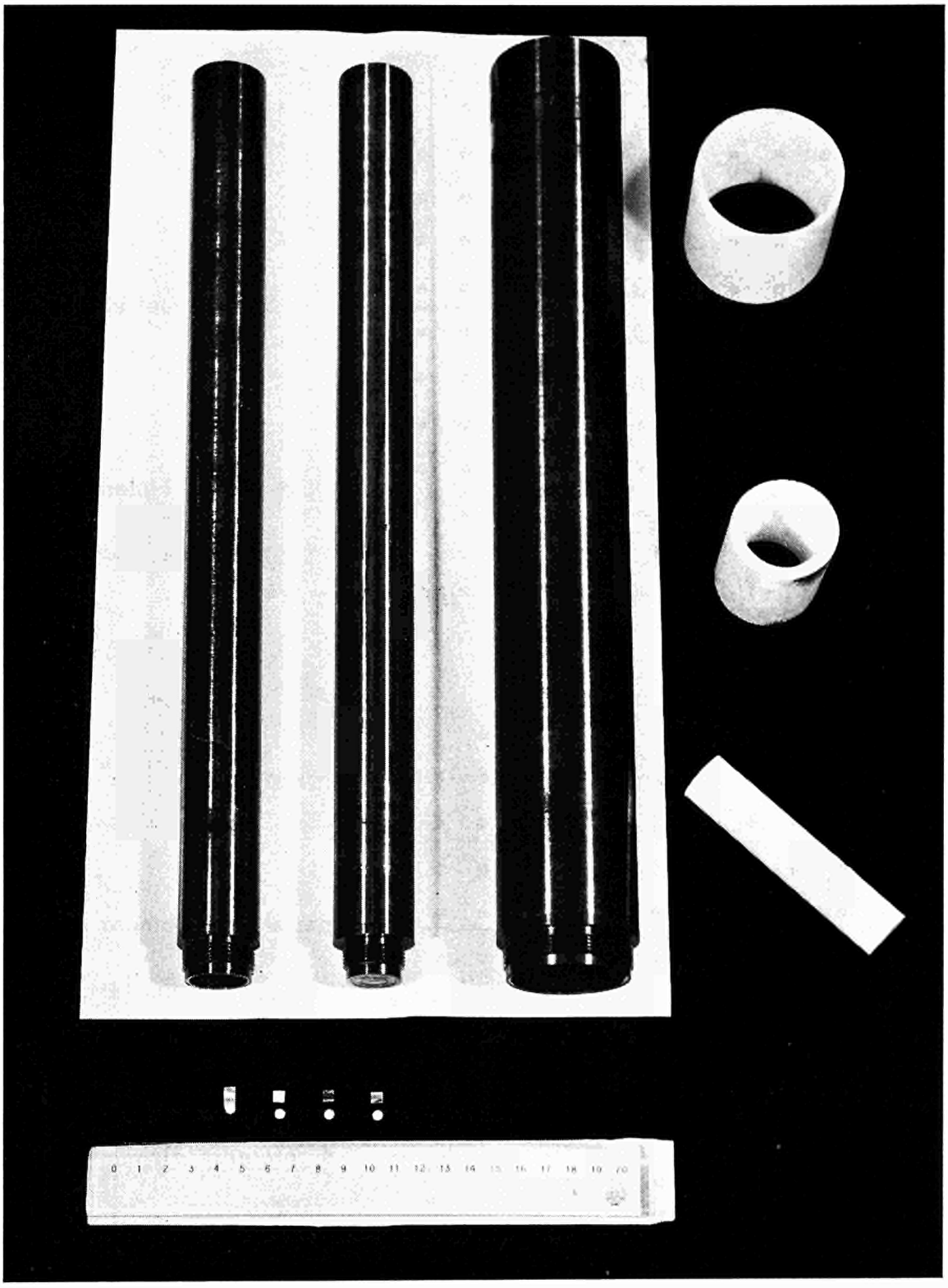

Fig. 8. — From left above: uranium slugs and polistyrene pieces.
Below: one aluminum holder opened three dysprosium detectors alongside aluminum holders (closed).

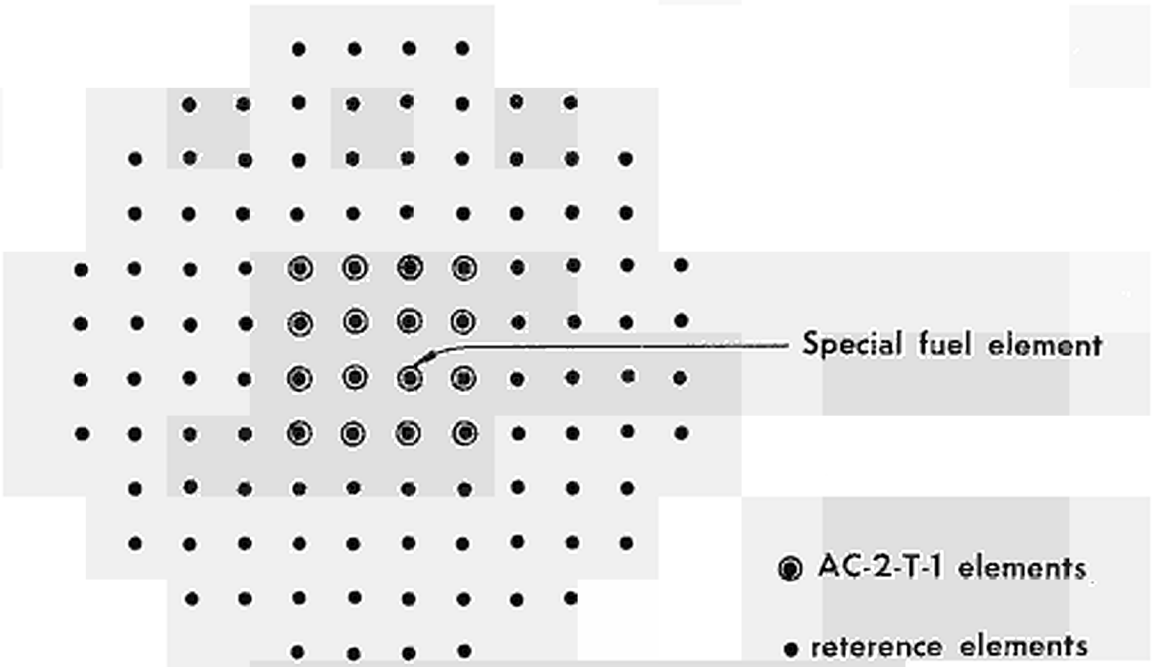

Fig. 9-a — *Core configuration for AC-2-T-1-21 fine flux measurement.*

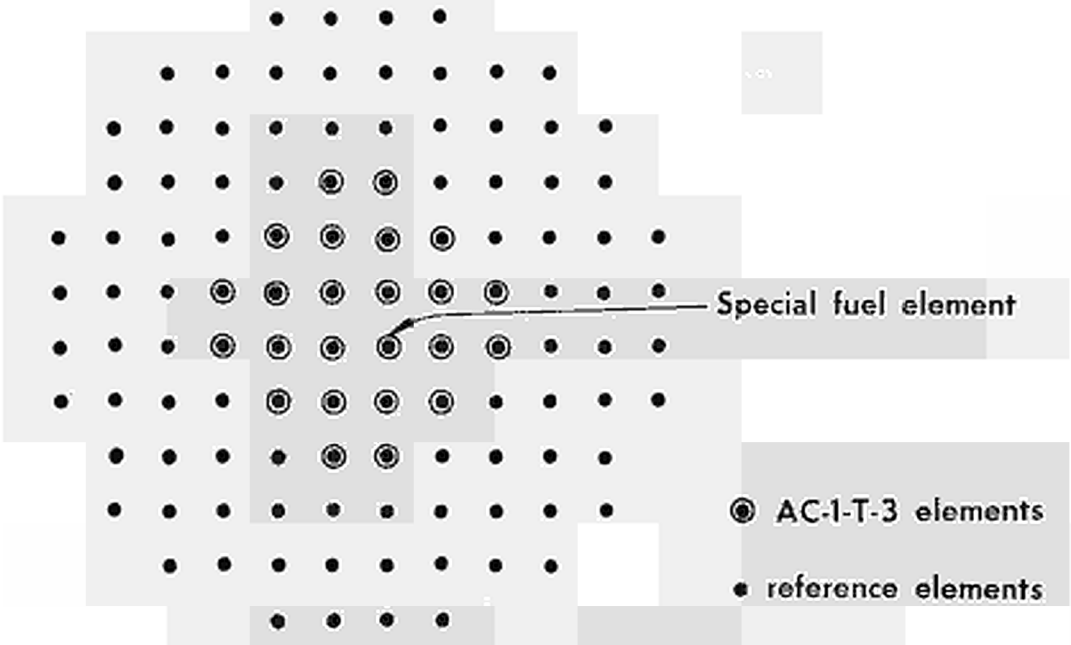

Fig. 9-b — *Core configuration for AC-1-T-3-24 fine flux measurement.*

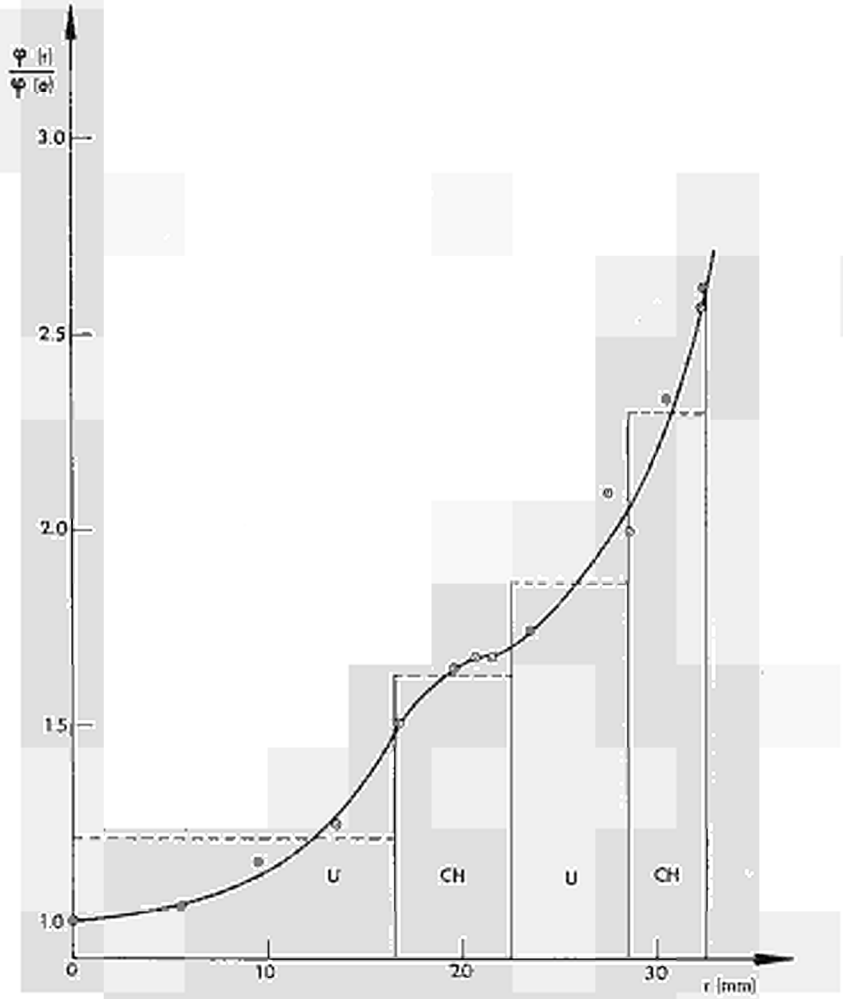

Fig. 10 — *AC-2-T-1-21 experimental flux distribution.*

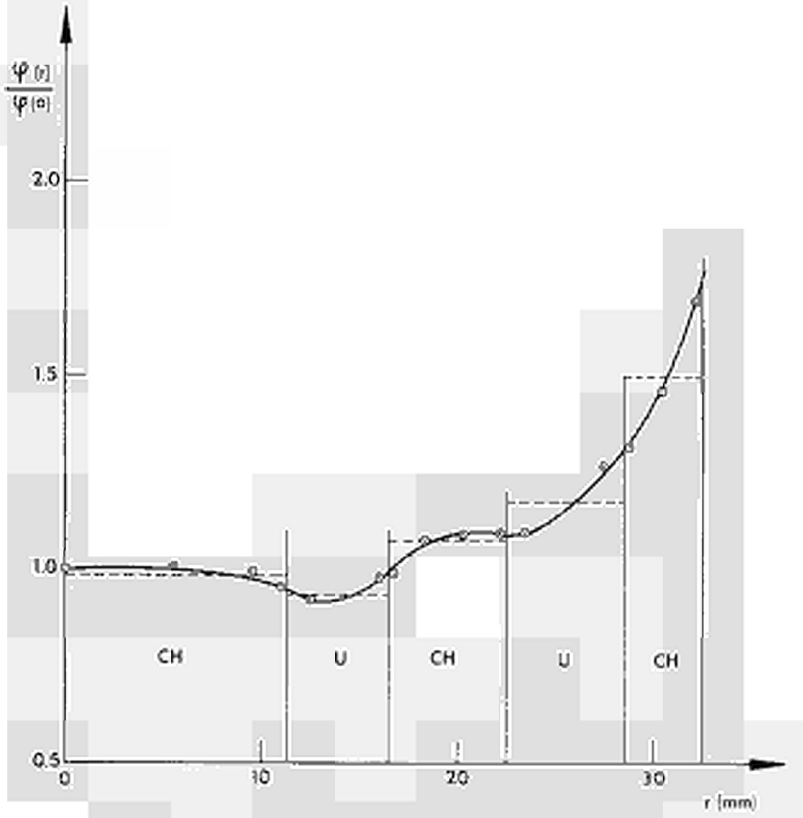

Fig. 11 — *AC-1-T-3-24 experimental flux distribution.*

CDNA00024ENC